Fluorescence correlation spectroscopy (IUPAC Technical Report)*

Jörg Enderlein‡

Third Institute of Physics–Biophysics, Georg-August-University, Göttingen, Germany

Abstract: We present an overview on the applicability of fluorescence correlation spectroscopy (FCS) for the accurate determination of translational diffusion coefficients and thus, via the Stokes–Einstein relation, of molecular size. We consider several of the most common sources of optical aberrations and their impact on the outcome of conventional FCS measurements. We describe also a new variant of FCS, dual-focus FCS, which is robust against most of the considered aberrations, and we report reference values of diffusion coefficients for several fluorescent dyes across the visible spectrum.

Keywords: diffusion coefficients; fluorescence; fluorescence intensity; fluorescence spectroscopy; IUPAC Analytical Chemistry Division; IUPAC Organic and Biomolecular Chemistry Division; IUPAC Physical and Biophysical Chemistry Division; Stokes–Einstein relation.

CONTENTS

I. INTRODUCTION

Fluorescence correlation spectroscopy (FCS) is the generalized name for a set of spectroscopic methods that are based on the measurement and correlation analysis of fluorescence intensity fluctuations originating from a small number of fluorescing molecules, usually contained within a sufficiently small detection region. Any process that influences the fluorescence intensity of these molecules (such as changes of their position within the measurements system, their photophysics, chemical reactions, conformational changes, etc.) will lead to a temporally changing fluorescence signal, most often in a sto-

chastic way. For example, molecules that are freely to diffuse in and out of the detection region will generate a stochastically changing fluorescence intensity signal. Similarly, molecules that, besides cycling through the first excited singlet and ground state, can switch from time to time into a nonfluorescent triplet state will generate a fluctuating fluorescence intensity signal. The important point is that the character of these fluorescence signal fluctuations is connected with the underlying physical processes and their parameters (such as the diffusion coefficient or photophysical rate constants). The core idea of FCS is to evaluate the observed intensity fluctuation in such a way that one can determine these parameters. The standard approach is to perform on the measured fluorescence intensity signal a second-order correlation analysis by calculating

$$g(\tau) = \langle I(t)I(t+\tau) \rangle \tag{1}$$

where $g(\tau)$ is the autocorrelation function (ACF), $I(t)$ is the fluorescence intensity at time t, and the triangular brackets denote averaging over all time values t. The physical meaning of the autocorrelation is that it is directly proportional to the probability of detecting a photon at time τ (the lag time) if there was a photon detection event at time zero. This probability is composed of two basically different terms. Firstly, the two photons detected at time zero and at time τ can originate from uncorrelated background or from different fluorescing molecules and therefore do not have any physical correlation (provided there is no interaction of the different fluorescing molecules). These events will contribute to a constant offset of $g(\tau)$ that is completely independent on τ (the joint probability to detect two physically uncorrelated photons is completely independent of the time distance between their detection). Secondly, the two photons can originate from one and the same molecule and are then physically correlated.

Let us start with some very simple qualitative considerations concerning the lag-time dependence of $g(\tau)$. Suppose a molecule is close to the centre of the detection volume. Then there will be a high probability of detecting a large number of consecutive fluorescence photons from this molecule, that is, the fluorescence signal will be highly correlated in time. When the molecule, owing to diffusion, starts to exit the detection volume, this correlation will continually decrease, namely, the probability to see further fluorescence photons will decrease in time until the molecule has completely diffused away and the correlation is completely lost. Of course, the temporal decay of the correlation, more precisely the characteristic time of the temporal decay of $g(\tau)$, will be proportional to the diffusion speed of the molecule: The larger the diffusion coefficient, the faster the fluorescence correlation decays.

A second important property of the ACF is its dependence on the concentration of fluorescing molecules. It is rather obvious that the fluorescence intensity fluctuations will be larger for smaller molecule concentrations. Indeed, if one has, on average, only a signal molecule within the detection volume, then the diffusion of this molecule out of this volume or the diffusion of another molecule into this volume will cause a big change in measured fluorescence intensity. On the contrary, if the average number of fluorescing molecules within the detection volume is rather large (e.g., several hundreds), then the leaving or entering of a molecule causes only small signal variations. Intuitively, one may expect a direct connection between the average number of molecules within the detection volume (i.e., concentration) and the amplitude of the fluorescence intensity fluctuations. And indeed, there is a direct connection between the inverse concentration of fluorescing molecules and the amplitude of the ACF.

Thus, FCS measurements can provide information about diffusion and concentration of fluorescing molecules. Any process that alters one (or both) of these quantities can also be measured by FCS. For example, consider the binding of two proteins in solution: by labeling one of the binding partners with a fluorescence label, and monitoring with FCS the changing value of the diffusion coefficient of the labeled molecules upon binding, one can directly measure binding affinities and kinetics.

On different time scales, the temporal behaviour of the ACF is determined by different properties of the fluorescing molecules: On a nanosecond time scale, photon anti-bunching can be observed, reflecting the fact that directly after the emission of a photon the molecule needs to get re-excited again to be able to emit the next photon, leading to a steep decrease of $g(\tau)$ towards short times. On a

microsecond time scale, $g(\tau)$ is dominated by triplet-state dynamics. If excitation and/or detection is performed with polarization filters, the autocorrelation will also show contributions from rotational diffusion dynamics of the molecules. On a millisecond-to-second level, the ACF shows a typical decay owing to the lateral diffusion of the molecules out of the detection region. The diffusion coefficient is also the parameter most frequently addressed by FCS measurements.

FCS was originally introduced by Elson, Magde, and Webb in the early 1970s [1–3]. In its original form it was invented for measuring diffusion, concentration, and chemical or biochemical interactions or reactions of fluorescent or fluorescently labeled molecules at nanomolar concentrations in solution. It took nearly two decades until, with the development of new lasers with high beam quality and temporal stability, low-noise single-photon detectors, and high-quality microscope objectives with nearly perfect imaging quality at high numerical aperture, the technique has seen a renaissance. Achieving values of the detection volume within the range of a few μm^3 made the technique applicable for samples at reasonably high concentrations and short measurement times.

The advantage of FCS is its relative simplicity. Its drawback is that it works only within a very limited concentration range: If the concentration of fluorescing molecules becomes too large (typically $\gg 10^{-8}$ M), then the contribution from correlated photons from individual molecules, scaling with the number N of molecules within the detection volume, becomes very small compared with the contribution by uncorrelated photons from different molecules, scaling with N^2. If the concentration is too low (typically $<10^{-13}$ M), then the probability of finding a molecule within the detection region becomes extremely low. In both cases, the measurement time for obtaining a high-quality ACF gets prohibitively large, although a remedy for that problem is to rapidly scan the laser focus through the solution [4,5].

There are numerous excellent reviews and overviews of FCS, see refs. [6–8], and there is even a complete book devoted to it [9]. The present note gives a very general introduction to the philosophy of FCS, trying to be self-contained, developing the fundamental principles of FCS, but also describing recent methodological advances that are not well covered by previous reviews. In what follows, the focus will be mainly on the application of FCS to precisely measured diffusion coefficients. This also allows a thorough discussion of the experimental set-up, potential optical problems, and the data evaluation.

II. OPTICAL SET-UP

A typical FCS measurement set-up is shown in Fig. 1 [10]. Fluorescent molecules are dissolved in an aqueous solution that is placed on top of a chambered cover slide. A collimated laser beam with perfect Gaussian TEM_{00} mode [11] is coupled via a dichroic mirror into an objective with high NA that focuses the laser into a diffraction-limited spot in the sample. The dichroic mirror is reflective at the laser's wavelength and transmissive at the wavelengths of the fluorescence emission. The use of a Gaussian TEM_{00} mode assures diffraction-limited focusing of light, thus achieving minimum focus diameter in the sample. Fluorescence light generated in the sample is collected by the same objective (so-called epifluorescence set-up), transmitted through the dichroic mirror, and focused onto a circular confocal aperture. Behind the aperture, the fluorescence light is refocused onto two sensitive light detectors, usually single-photon avalanche diodes (SPADs). The confocal aperture effectively rejects fluorescence light that is generated outside the focal plane. In combination, fluorescence generation (by diffraction-limited focusing of excitation light) and fluorescence detection (by confocal detection) generate an effective detection volume of ca. 0.5 µm in diameter in the focal plane and a few micrometers along the optical axis.

Using two detectors is important for efficient elimination of the effects of SPAD dead-time and after pulsing on an ACF. Usually, detector dead times are in the range of several tens to hundreds nanoseconds. They cause the measured ACF to drop towards zero at lag times that are comparable with the detector's dead time. Detector after-pulsing is the effect that a genuine photon detection pulse is fol-
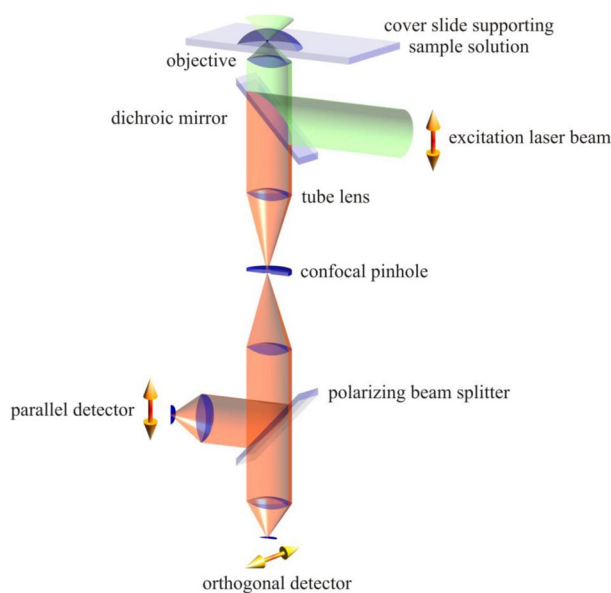
Fig. 1 Principal scheme of a confocal epi-fluorescence microscope as used in FCS. Shown is a set-up with a linearly polarized excitation laser. Detection is done within two detection channels after splitting the light with a polarizing beam splitter. The detectors are usually SPADs or photomultiplier tubes. The vertical position of the objective can be accurately adjusted using a piezo actuator (not shown).

lowed by a so-called after-pulse with a delay between microseconds to seconds. The origin of after-pulsing in SPADs is as follows: a primary photoelectron initiates an avalanche of ionizations that causes a breakdown pulse at the detector output. Some of the generated charge carriers may become temporarily trapped and afterwards released by thermal excitation, so that new charge carriers are created that lead to after-pulses which are correlated with the initial event. The probability of after-pulsing depends on many different parameters like material defects, temperature, and operating conditions of the detector. The process of after-pulsing becomes typically visible as a fast decay of the ACF at microsecond lag times. By using two detectors and correlating only photons from different detectors, both the effects of dead time as well as after-pulsing are successfully eliminated when calculating an ACF.

The exact shape and size of that detection volume determine the shape and temporal decay of the ACF. For example, the smaller the detection volume, the faster molecules diffuse out and the faster the ACF decays, and vice versa. The actual quantity that defines the ACF is the so-called molecule detection function (MDF). The MDF describes the chance of seeing a fluorescence photon from a molecule at a given position $\mathbf{r}$ in the sample. Thus, the MDF, which we will denote by $U(\mathbf{r})$, is a function of position $\mathbf{r}$ and rapidly falls off to zero if one moves away from the optical axis and/or the focal plane. As we will see below, knowing the exact shape of the MDF allows one to calculate exactly the shape of the ACF, which can then subsequently be used to fit experimental data for obtaining, for example, diffusion and/or concentration values of the fluorescent molecules. However, this is also the principal problem of FCS: a precise quantitative evaluation of an ACF critically depends on the exact knowledge of the MDF. This is discussed in detail in Section IV.

III. DATA ACQUISITION AND EVALUATION

Conventional FCS set-ups were used to employ hardware autocorrelators that calculated the ACF onboard on the basis of the signal from the photodetectors. Recently, most set-ups use fast photon-counting electronics for asynchronously recording and storing the arrival times of the detected photons, and subsequently use software algorithms for calculating the ACF from the recorded photon data. This permits much more flexibility in data handling and evaluation, as will be seen, for example, in the case of fluorescence lifetime correlation spectroscopy, and we will describe this approach here in more detail.

Asynchronously measured single-photon counting data consist of a linear file of detection times $(t_1, t_2, ..., t_N)$ of the detected photons, where N is the total number of detected photons during a given measurement. A special feature of these detection times is that they are integer multiples of some minimal time δt, determined by the temporal resolution of the detection electronics. Without restriction of generality, it can be assumed that all times are measured in units of δt, so that all the numbers t_j take integer values. The value $g(\tau)$ of the ACF for a given lag time τ is defined in eq. 1. For a photon detection measurement with temporal resolution δt, the intensity values $I(t)$ within consecutive time intervals can only take the values $1/\delta t$ or 0, depending on whether there was a photon detection event during a time interval of width δt or not. The average value from eq. 1 is then calculated as the sum over all consecutive time intervals of width δt, divided by the total number of intervals. In practice, one does not compute the ACF for all possible values of lag time τ, but at increasingly spaced lag-time values. If the temporal resolution of the photon detection is, for example, 100 ns, and one desires to follow correlation processes up to a minute, possible values of lag time τ are any value between 100 ns and 60 s in intervals of 100 ns, resulting in 6×10^8 possible lag-time values. Calculation of $g(\tau)$ for all of these values would be an enormously time-consuming numerical effort. Instead, the autocorrelation is calculated for only a few approximately logarithmically spaced values of τ.

A straightforward way of calculating the ACF is to divide the total measurement time, $t_N - t_1$, into intervals of unit length δt, and to sort the detected photons into these intervals corresponding to their arrival times t_j. The result is a synchronous photon detection intensity file I_j with j running from 1 through $t_N - t_1$, where I_j can only adopt the values 1 or 0. The fluorescence autocorrelation can then be calculated as given by eq. 1. In practice, such an approach is prohibitively demanding of memory and computationally expensive. An alternative, and much more efficient, FCS algorithm works directly on the arrival times $(t_1, t_2, ..., t_N)$, without converting them into time-binned data. For a given lag time τ, the algorithm searches for all photon pairs in the data stream that are a temporal distance τ apart from each other. The number of photon pairs with a distance τ is directly proportional to the autocorrelation value at lag time τ. The technical details of the algorithm are given ref. [12].

IV. MEASURING DIFFUSION AND CONCENTRATION

Thermally induced translational diffusion is one of the fundamental properties exhibited by molecules within a solution. Via the Stokes–Einstein relation, it is directly coupled with the hydrodynamic radius of the molecules [13]. Any change in that radius will change the associated diffusion coefficient of the molecules. Such changes occur to most biomolecules—in particular, proteins, RNA, and DNA—when interacting with their environment (e.g., binding of ions or other biomolecules) or performing biologically important functions (such as enzymatic catalysis) or reacting to changes in environmental parameters such as pH, temperature, or chemical composition (like protein unfolding). Therefore, the ability to precisely measure diffusion coefficients has a large range of potential applications, such as monitoring conformational changes in proteins upon ion binding or unfolding. However, many biologically relevant conformational changes are connected with rather small changes in hydrodynamic radius on the order of 0.1 nm (e.g., see [14]). To monitor these small changes, it is necessary to measure the diffusion coefficient with an accuracy of better than a few percent. Standard methods for diffusion coef-

ficient measurements achieving this accuracy are dynamic light scattering (DLS) [15], pulsed-field gradient NMR [16], size-exclusion electrophoresis [17], or analytical ultracentrifugation [18]. However, all these methods operate at rather high sample concentrations, far away from the limit of infinite dilution. For obtaining the correct infinite-dilution limit and thus a correct estimate of the hydrodynamic radius, one has often to measure at different concentrations and to extrapolate the concentration/diffusion coefficient curve towards zero concentration (see, e.g., [19]). Another problem is that proteins are often prone to aggregation [20] at the concentrations needed for obtaining sufficient data quality. Thus, FCS is a relatively simple and attractive alternative for measuring diffusion coefficients, and the next sections will explain in detail how this is done.

IV.1 One-focus FCS

Following eq. 1, the ACF is the correlation of the fluorescence intensity with a time-shifted replica of itself, calculated for all possible lag times τ. The measured signal $I(t)$ stems from the fluorescence of all the molecules within the sample plus uncorrelated background I_{bg} (light scattering, electronic noise, etc.)

$$I(t) = I_{bg} + \sum_j I_j(t) \tag{2}$$

where the index j refers to the jth molecule, and the summation runs over all molecules in the sample. Thus, the ACF $g(\tau)$ is given by

$$g(\tau) = \left\langle \left(I_{bg}(t) + \sum_j I_j(t) \right) \left(I_{bg}(t+\tau) + \sum_j I_j(t+\tau) \right) \right\rangle$$
$$= \sum_j \left\langle I_j(t) I_j(t+\tau) \right\rangle + \sum_{j \neq k} \overline{I}_j \overline{I}_k + \sum_j \overline{I}_j \overline{I}_{bg} + \overline{I}_{bg}^2 \tag{3}$$

where the triangular brackets and bars denote averaging over all possible time values t. In the last line, it was taken into account that fluorescence photons coming from different molecules are completely uncorrelated (no intermolecular interaction provided). Because all molecules in solution are indistinguishable, the last equation can be simplified further to

$$g(\tau) = N \left\langle i(t) i(t+\tau) \right\rangle + N(N-1) \left\langle i(t) \right\rangle^2 + N \left\langle i(t) \right\rangle \overline{I}_{bg} + \overline{I}_{bg}^2 \tag{4}$$

where i is the measured fluorescence intensity of *any* molecule, and N is the total number of molecules present in the sample. Thus, the task of calculating the function $g(t)$ reduces to calculating $\langle i(t) i(t+\tau) \rangle$, the correlation of the fluorescence signal from one and the same molecule, and $\langle i(t) \rangle$, the average detected fluorescence intensity of one molecule.

The correlation $\langle i(t) i(t+\tau) \rangle$ of the fluorescence signal from one and the same molecule can be easily derived when remembering its physical meaning: It is proportional to the chance of seeing, from one and the same molecule, a photon at time $t + \tau$ if there was a photon detection at time t. The probability of finding a molecule within an infinitely small volume dV anywhere in the sample is equal to dV/V, where V is the total sample volume. Next, the probability to detect a photon from a molecule at a given position $\mathbf{r}_0$ is directly proportional to the value of the MDF at this position, i.e., to $U(\mathbf{r}_0)$. Furthermore, the chance that the molecule diffuses from position $\mathbf{r}_0$ to position $\mathbf{r}_1$ within time τ is given by the solution of the diffusion equation

$$\frac{\partial G}{\partial \tau} = D \Delta G \tag{5}$$

where Δ is the three-dimensional Laplace operator in coordinate $\mathbf{r}_1$, D is the diffusion coefficient of the molecule, and G approaches a three-dimensional Dirac function for $\tau \to 0$, $G(\mathbf{r}_1, \mathbf{r}_0, \tau = 0) = \delta$, i.e., the molecule is exactly at position $\mathbf{r}_0$ at time 0. For a sample with far removed boundaries, this solution is explicitly given by

$$G(\mathbf{r}_1, \mathbf{r}_0, t) \equiv G(\mathbf{r}_1 - \mathbf{r}_0, t) = \frac{1}{(4\pi D\tau)^{3/2}} \exp\left[-\frac{|\mathbf{r}_1 - \mathbf{r}_0|^2}{4D\tau} \right] \tag{6}$$

Finally, the chance to detect a photon from the molecule at the new position $\mathbf{r}_1$ is again proportional to the value of the MDF at this position, i.e., to $U(\mathbf{r}_1)$. Thus, the autocorrelation $\langle i(t)i(t+\tau)\rangle$ is calculated as the product of all these individual contributions and averaging over all possible initial and final positions of the molecule, i.e., integrating over $\mathbf{r}_0$ and $\mathbf{r}_1$

$$\langle i(t)i(t+\tau)\rangle = \frac{1}{V} \int_V d\mathbf{r}_1 \int_V d\mathbf{r}_0 \, U(\mathbf{r}_1) G(\mathbf{r}_1, \mathbf{r}_0, \tau) U(\mathbf{r}_0) \tag{7}$$

Similarly, the average fluorescence intensity from a single molecule in the sample is given by

$$\langle i(t)\rangle = \frac{1}{V} \int_V d\mathbf{r}\, U(\mathbf{r}) \tag{8}$$

so that the full ACF, in its most general form, reads

$$g(\tau) = c \int_V d\mathbf{r}_1 \int_V d\mathbf{r}_0 \, U(\mathbf{r}_1) G(\mathbf{r}_1, \mathbf{r}_0, \tau) U(\mathbf{r}_0) + \left[\overline{I}_{bg} + c \int_V d\mathbf{r}\, U(\mathbf{r}) \right]^2 \tag{9}$$

where c denotes the concentration of fluorescent molecules (numbers per volume) and one has used the fact that in the limit of large sample volume $N/V \to c$ and $N(N-1)/V^2 \to c^2$.

The above eqs. 7 and 8 are of general validity, but before being able to apply them to the evaluation of real FCS experiments one has to specify the MDF $U(\mathbf{r})$. In the majority of publications on FCS, one has adopted a very simple approximation of the MDF, assuming that it is well described by a three-dimensional Gaussian distribution, i.e.

$$U(\mathbf{r}) = \kappa \exp\left[-\frac{2}{a^2}(x^2 + y^2) - \frac{2}{b^2} z^2 \right] \tag{10}$$

where κ is some overall constant, (x, y, z) are Cartesian coordinates centred at the intersection of focal plane and optical axis and with $x = y = 0$ being the optical axis, and a and b are the characteristic half axes of the cylindrically symmetric, Gaussian-shaped detection volume. This corresponds to the lowest-order polynomial expansion of $\ln U(\mathbf{r})$ (due to axial and mirror symmetry, terms linear in x, y, z are absent). The characteristic parameters a and b are not known a priori and are usually determined by reference measurements on a sample with known diffusion coefficient. Using the expression of eq. 10, the autocorrelation $\langle i(t)i(t+\tau)\rangle$ can now be explicitly calculated as

$$\begin{aligned} \langle i(t)i(t+\tau)\rangle &= \frac{c\varepsilon^2}{(4\pi Dt)^{3/2}} \int_V d\mathbf{r} \int_V d\boldsymbol{\rho}\, U(\mathbf{r}+\boldsymbol{\rho}) \exp\left(-\frac{|\boldsymbol{\rho}|^2}{4Dt} \right) U(\mathbf{r}) \\ &= \left(\frac{\pi^{3/2}}{8} \right) \frac{c\varepsilon^2 a^2 b}{(1 + 4Dt/a^2)\sqrt{1 + 4Dt/b^2}} \end{aligned} \tag{11}$$

where ε is a constant factor taking into account overall detection efficiency of the measurement system, absolute fluorescence brightness of the molecules (defined by the product of absorption cross-section and fluorescence quantum yield), etc. In a similar way, the average fluorescence signal is given by

$$\langle i(t) \rangle = c\varepsilon \int_V d\mathbf{r} U(\mathbf{r}) = \left(\frac{\pi^3}{8}\right)^{1/2} c\varepsilon a^2 b \tag{12}$$

Thus, the final result for the total autocorrelation reads

$$g(\tau) = \left(\frac{\pi^{3/2}}{8}\right) \frac{c\varepsilon^2 a^2 b}{\left(1 + 4D\tau/a^2\right)\sqrt{1 + 4D\tau/b^2}} + \left[\bar{I}_{bg} + \left(\frac{\pi^3}{8}\right)^{1/2} c\varepsilon a^2 b\right]^2 \tag{13}$$

An important property of the ACF is that the concentration of the fluorescent species can be derived from eq. 13 via

$$\frac{g(\infty)}{g(0) - g(\infty)} = c \frac{\left[\int d\mathbf{r} U(\mathbf{r}) + \bar{I}_{bg}\right]^2}{\int d\mathbf{r} U^2(\mathbf{r})} \tag{14}$$

where we have taken into account that G($\boldsymbol{\rho},\tau$) in eq. 6 approaches a Dirac function for $\tau \to 0$. Using eq. 14, one can define the *effective detection volume* V_{eff} as

$$V_{eff} = \frac{\left[\int d\mathbf{r} U(\mathbf{r})\right]^2}{\int d\mathbf{r} U^2(\mathbf{r})} \tag{15}$$

so that, for negligible background, the left-hand side of eq. 14 equals cV_{eff} (i.e., the mean particle number within V_{eff}). Thus, the ACF is often used for estimating concentrations of fluorescing molecules.

Although eq. 13 is remarkably successful in fitting measured autocorrelation curves, the physical meaning of the parameters a and b is rather obscure, because the actual MDF is usually much more complicated than as given by eq. 10. The real shape of the MDF is only poorly described a three-dimensional Gaussian, see Fig. 2.

A more serious problem is that the exact form of the MDF is extremely sensitive to several optical and photophysical artifacts and can easily change from one measurement to another [21]. The most severe of them shall be discussed here. The first common problem is that state-of-the-art water immersion objectives used in FCS set-ups are designed to image through a cover slide of a specific thickness. In this sense, the cover slide acts as the last optical element of an objective, and the optical quality of imaging (and laser focusing) critically depends on the exact matching between the cover slide thickness the objective is adjusted to and its actual thickness. What happens when the cover slide thickness deviates from its design value by only a few micrometers is shown in Fig. 3, where one can see the severe optical aberrations introduced by cover slide thickness mismatch and the resulting deformation of an ACF and the shift of its decay towards longer lag times. The enlargement of the MDF results in increased diffusion times, i.e., apparently lower diffusion coefficients, and in an apparently increased concentration (there are more molecules present in the detection volume because the latter has become larger). In general, any aberration results in an increased detection volume and thus leads to the same trend of an apparently lower diffusion coefficient and higher concentration with increasing aberration. The impact on the apparent concentration is much stronger than on the apparent diffusion, resulting, for a cover slide thickness deviation of 10 μm, in an error of over 100 % for the first and roughly 30 % for the second. It should be noted that the errors shown do not change significantly when changing the focus position in the solution.
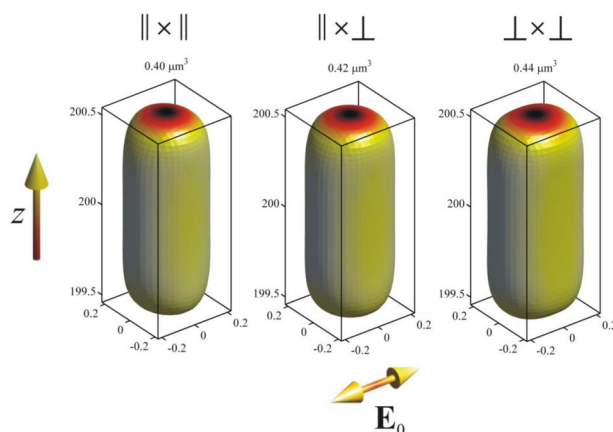
Fig. 2 Shape of the MDF for three different detection and correlation schemes, visualized by displaying the iso-surfaces where the MDF has fallen to $1/e^2$ (~13 %) of its maximum value in the centre. The left-hand box shows the MDF of the autocorrelation of the detector signal monitoring fluorescence polarization parallel to the incident laser beam. The right-hand box shows that of the detector signal monitoring fluorescence polarization perpendicular to the incident laser beam. The middle box shows the MDF for the cross-correlation between both detectors. The extreme case of completely anisotropic molecules was studied (where the maximum impact of polarization effects on the ACF is expected). Vertical axis (z) is the optical axis; all units are given in micrometers, $z = 0$ is at the surface of the cover slide. Shown is also the polarization of the incident laser beam ($\mathbf{E}_0$). Shading of the iso-surfaces indicates distance from the optical axis. The differences between the three above figures are subtle, resulting in nearly identical ACF curves. Thus, in practice, one may safely neglect the effects of polarized detection when being concerned with the diffusional part of an ACF [21].
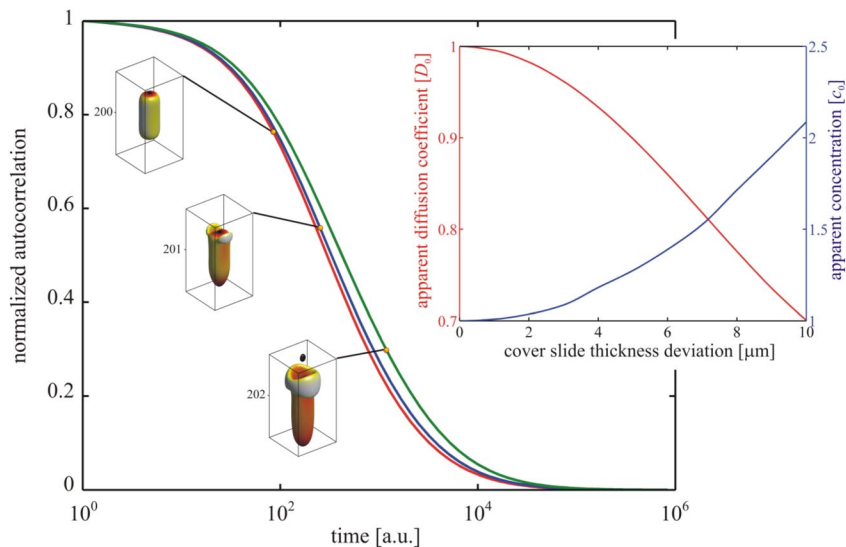

Fig. 3 The large figure shows, from left to right, the MDF and ACF for three increasing values of cover slide thickness deviation, $\delta = 0$, $\delta = 5$ μm, and $\delta = 10$ μm. Box size of the MDF displays is $1 \times 1 \times 2$ μm^3; the number next to the box gives the centre position along the optical axis in μm. Note the shift of the centre of the MDF along the optical axis for increasing values of δ. The inset figure shows the dependence of apparent diffusion coefficient and the chemical concentration on thickness deviation value. These values would be obtained when performing a comparative FCS measurement using an ideal ACF ($\delta = 0$) as reference (same for following figures).

This is in stark contrast to the effect of refractive index mismatch, which is considered next. An optical microscope using a water immersion objective is optimally corrected for imaging in water. However, in many biophysical applications, one has to work in buffer solutions with slightly different refractive indices. Also, when measuring in cells or tissues, one faces similarly slight refractive index variations. Typical values of interest are between 1.333 and 1.360. Figure 4 shows the impact of refractive index mismatch on the MDF and ACF and subsequently on the apparent diffusion coefficient and concentration. The impact of even a slight refractive index mismatch is much more dramatic than that of cover slide thickness. This is mostly due to the large assumed distance of the focus position from the cover slide surface (200 μm, the default value of commercial instruments such as the Zeiss Confocor I). In contrast to cover slide thickness, the aberrations introduced by refractive index mismatch accumulate with increasing distance of the focus from cover slide surface because an increasingly thicker layer of solution with mismatched refractive index lies between the optics and the detection volume. The effect of refractive index mismatch can be much reduced by positioning the detection volume closer to the surface.
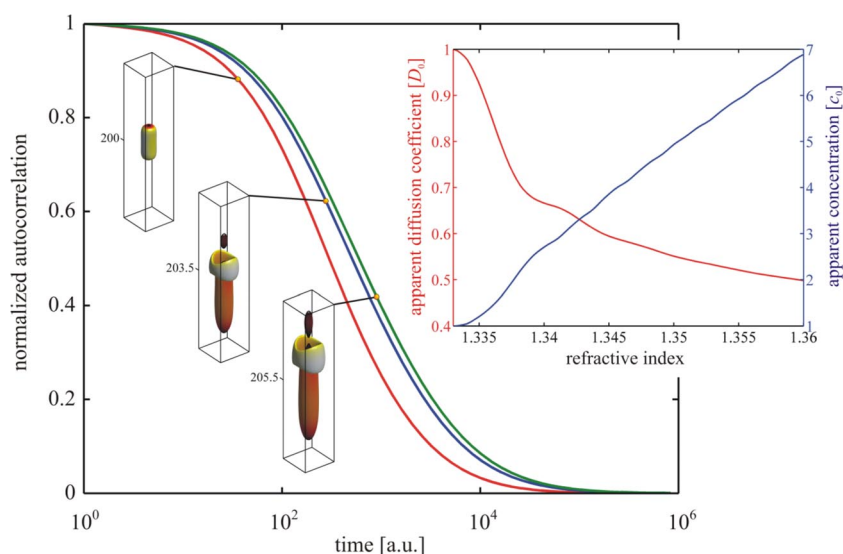

Fig. 4 The large figure shows, from left to right, the MDF and ACF for three increasing values of refractive index of the sample solution, $n_m = 1.333$, $n_m = 1.346$, and $n_m = 1.360$. Box size of the MDF displays is $1 \times 1 \times 5$ μm^3. Note again the shift of the centre of the MDF along the optical axis for increasing values of n_m. The inset figure shows the dependence of apparent diffusion coefficient and the concentration on refractive index.

Another purely optical effect is laser beam astigmatism, i.e., different focus positions within different axial planes of the laser beam. Astigmatism is easily introduced by slight curvatures of reflective elements in the optical set-up (such as the dichroic mirror), or by slight axial asymmetry of the optical fire that is often used for guiding the excitation light towards the objective.

The impact of astigmatism on the shape of the MDF and ACF, as well as the apparent diffusion coefficient and chemical concentration, is shown in Fig. 5. As can be seen, the effect of astigmatism on measured diffusion and concentration is of similar magnitude to that of cover slide thickness deviation. As for cover slide thickness, the effect of astigmatism is rather independent of focus position in the sample.

A particularly intriguing effect in FCS measurements is the dependence of the ACF on excitation intensity due to optical saturation. Optical saturation occurs when the excitation intensity becomes so large that a molecule spends more and more time in a non-excitable state, so that increasing the excita-
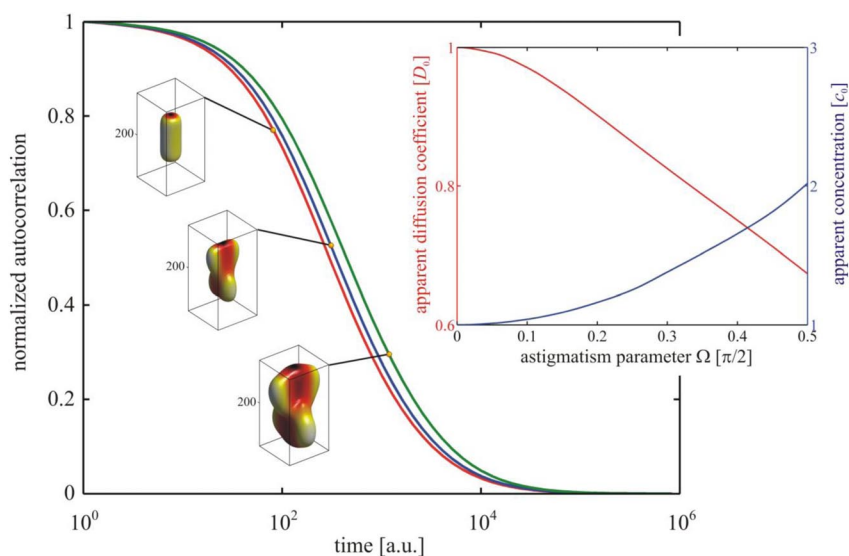
Fig. 5 The large figure shows, from left to right, the MDF and ACF for three increasing values of laser beam astigmatism (for definition of astigmatism, see ref. [21]). The box size of the MDF displays is $1 \times 1 \times 2 \, \mu m^3$. There is no shift of the centre of the MDF along the optical axis for increasing values of astigmatism. The inset figure shows the dependence of the apparent diffusion coefficient and the concentration on beam astigmatism.

tion intensity does not lead to a proportional increase in emitted fluorescence intensity [22]. The most common sources of optical saturation are (i) excited-state saturation (i.e., the molecule is still in the excited state when the next photon arrives); (ii) triplet-state saturation (i.e., the molecule undergoes intersystem-crossing from the excited to the triplet state so that it can no longer become excited until it returns back to the ground state); (iii) other photoinduced transitions into a nonfluorescing state, such as the photoinduced *cis–trans*-isomerization in cyanine dyes, or the optically induced dark states in quantum dots. The exact relation between fluorescence emission intensity and excitation intensity can be very complex [22] and even dependent on the excitation mode (pulsed or continuous wave), but a sufficiently good approximation of the dependence of fluorescence intensity on excitation intensity is given by the simple relation

$$I_{\text{fluo}} \propto \frac{I_{\text{exc}}}{1 + I_{\text{exc}} / I_{\text{sat}}} \tag{16}$$

where I_{fluo} and I_{exc} are the fluorescence and excitation intensity, respectively, and I_{sat} is a parameter called the saturation intensity which describes the saturation behaviour of a given dye. Figure 6 shows how optical saturation changes the shape of the MDF and ACF and the apparent diffusion coefficient and concentration. An important feature is the behaviour of the curves of apparent diffusion and concentration in the limit of vanishing excitation intensity: Whereas for all optical effects studied before the slope of these curves tended to zero for vanishing aberration (or astigmatism), its absolute value now is largest at zero intensity.

To better understand the reason for that behaviour, consider an ideal Gaussian excitation profile $I_0 \cdot \exp(-x^2/2\sigma^2)$ with mean square deviation of one. Figure 7 shows the widening of such a profile when transformed by a saturation to $I_0 \cdot \exp(-x^2/2\sigma^2)/[1 + I_0 \cdot \exp(-x^2/2\sigma^2)]$. As can be seen, relative change in profile width is fastest in the limit of zero intensity $I_0 \to 0$, explaining why one sees most of the changes in FCS at low saturation levels.
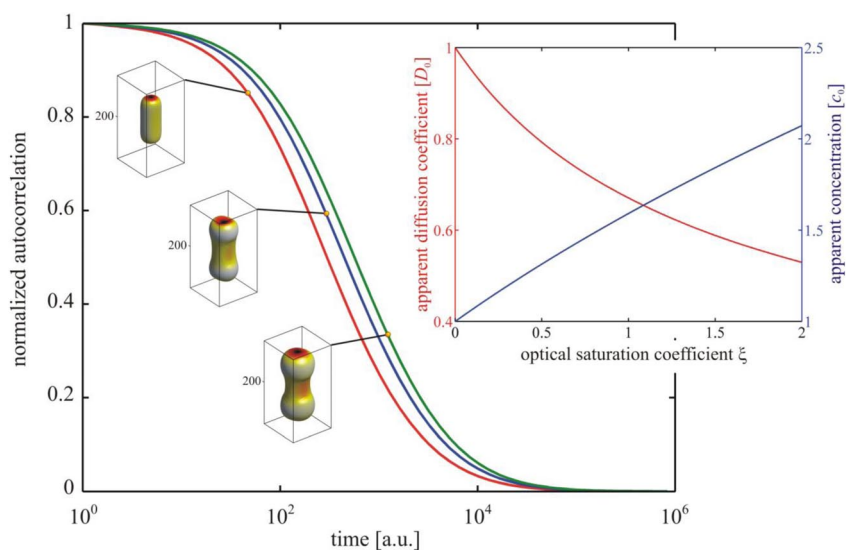
Fig. 6 The large figure shows, from left to right, the MDF and ACF for three increasing values of optical saturation, $\zeta = 0$, $\zeta = 1$, and $\zeta = 2$, where ζ is the maximum of I_{exc}/I_{sat}. The box size of the MDF displays is $1 \times 1 \times 2 \ \mu m^3$. The inset figure shows the dependence of apparent diffusion coefficient and concentration on optical saturation, i.e., excitation intensity.
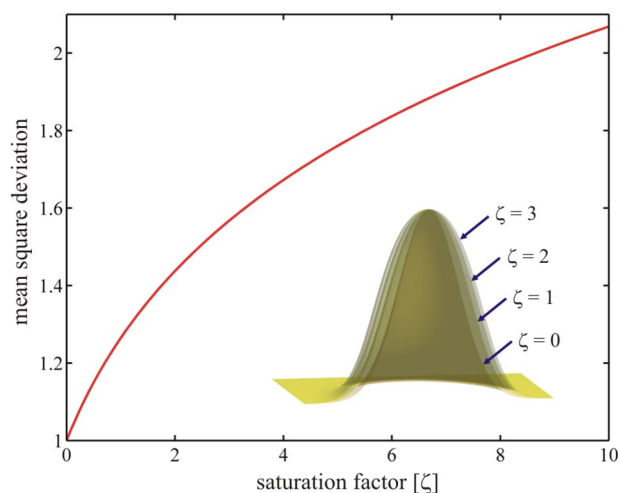

Fig. 7 Change of the mean-square deviation of the distribution $\exp(-x^2/2)/[1 + \zeta \cdot \exp(-x^2/2)]$ with increasing value of ζ.

All these effects make a quantitative evaluation of standard FCS measurements quantitatively unreliable. As pointed out before, the core problem is the absence of an extrinsic and fixed length scale in the experiment. Even referential measurements, i.e., using a dye with known diffusion coefficient for determining the parameters a and b and then using them to measure the diffusion of a sample, can be problematic owing to the strong dependence of an FCS result on optical saturation, which is itself determined, in a complex manner, by the photophysics of a particular dye. Even worse, the photophysical parameters of one and the same dye can change upon binding it to a protein or other target molecule! The next section describes a recent modification of the standard FCS measurement that seems to solve

this long-standing problem, and that allows for reproducible, quantitative, and absolute measurements of diffusion coefficients.

IV.2 Dual-focus FCS

Recently, a new and straightforward modification of FCS was developed [23], namely, dual-focus FCS or 2fFCS, that fulfils two requirements: (i) it introduces an external ruler into the measurement by generating two overlapping laser foci of precisely known and fixed distance, (ii) it generates the two foci and corresponding detection regions in such a way that the corresponding MDFs are sufficiently well described by a simple two-parameter model yielding accurate diffusion coefficients when applied to 2fFCS data analysis. Both these properties allow for measuring absolute values of the diffusion coefficient with an accuracy of a few percent. Moreover, the new technique is robust against refractive index mismatch and optical saturation effects, which are troubling to standard FCS measurements.

The 2fFCS set-up, as shown in Fig. 8, is based on a standard confocal epi-fluorescence microscope as was shown in Fig. 1. However, instead of using a single excitation laser, the light of two identical, linearly polarized pulsed diode lasers is combined by a polarizing beam splitter. Both lasers are pulsed *alternately* with a high repetition rate (ca. 40–80 MHz) and excitation scheme, which is called pulsed interleaved excitation or PIE [24]. Both beams are then coupled into a polarization-maintaining, single-mode fire. At the output, the light is again collimated. Thus, the combined light consists of a train of laser pulses with alternating orthogonal polarization. The beam is then reflected by a dichroic mirror towards the microscope's water-immersion objective, but before entering the objective, the light
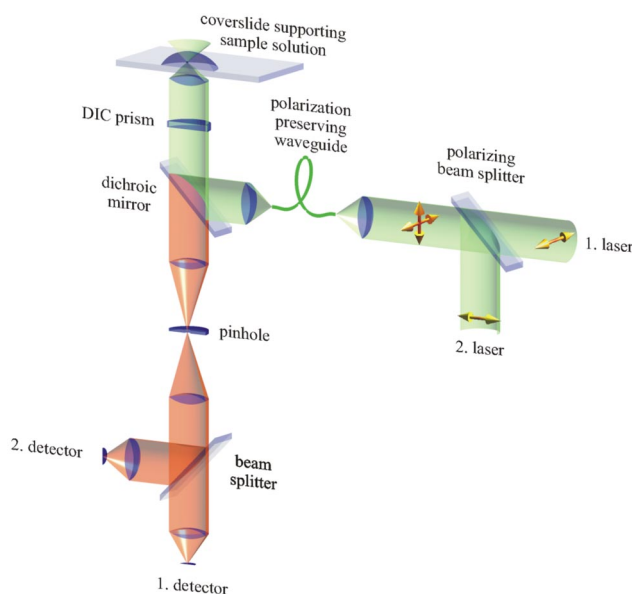

Fig. 8 Schematic of the 2fFCS set-up. Excitation is done by two interleaved pulsed lasers of the same wavelength. The polarization of each laser is linear but orthogonal to each other. Light is then combined by a polarizing beam splitter and coupled into a polarization maintaining optical single-mode fire. After exiting the fire, the laser light is collimated by an appropriate lens and reflected by a dichroic beam splitter through a DIC prism. The DIC prism separates the laser light into two beams according to the polarization of the incoming laser pulses. The microscope objective focuses the two beams into two laterally shifted foci. Fluorescence is collected by the same objective. The tube lens focuses the detected fluorescence from both excitation foci on a single pinhole. Subsequently, the fluorescence light is split by a 50/50 beam splitter and detected by two SPADs.

beam is passed through a Nomarski prism that is normally exploited for differential interference contrast (DIC) microscopy. The Nomarski prism is an optical element that deflects the laser pulses into two different directions according to their corresponding polarization. Thus, after focusing the light through the objective, two overlapping excitation foci are generated, with a small lateral shift between them. The distance between the beams is uniquely defined by the chosen Nomarski prism and is independent of the sample's refractive index, cover slide thickness, and laser beam astigmatism, because all these properties may introduce severe aberrations, but will not change the main distance between the axes of propagation of both focused laser beams.

As in one-focus FCS, the generated fluorescence is collected by the same objective, passed through the Nomarski prism and the dichroic mirror, and focused onto a single circular aperture (diameter 200 μm) which is positioned symmetrically with respect to both focus positions and chosen to be large enough to easily pass the light from both foci. After the pinhole, the light is collimated, split by a nonpolarizing beam splitter cube, and focused onto two SPADs. A single-photon counting electronics unit is used to record the detected photons from both SPADs with picosecond temporal resolution. The picosecond temporal resolution is used to decide which laser has excited which fluorescence photon, i.e., within which laser focus/detection volume the light was generated. This is done by correlating the detection time of each photon with the time of the last preceding laser pulse. In the data evaluation, all photons that fall into the first time window are associated with the first laser, and all photons that fall into the second time window with the second laser. For a successful working of that method it is, of course, necessary that the time between laser pulses is significantly larger than the fluorescence lifetime of the fluorescent molecules. Knowing which photon was generated in which detection volume, ACFs for each detection volume as well as cross-correlation function (CCF) between the two detection volumes can be calculated. The CCF is calculated in a similar way as the ACF but correlating photons only from different detection volumes. The CCF at lag time τ is thus proportional to the chance of seeing a photon from the second detection volume at any time $t + \tau$ if there was a detection event from the first detection volume at time t and vice versa.

A crucial point for a successful 2fFCS data analysis is to have a sufficiently appropriate model function for the MDF. It was found [23] that a suitable expression is given by the expression

$$U(\mathbf{r}) = \frac{\kappa(z)}{w^2(z)} \exp\left[-2\frac{x^2 + y^2}{w^2(z)}\right] \tag{17}$$

where $\kappa(z)$ and $w(z)$ are functions of the axial coordinate z (optical axis) defined by

$$w(z) = w_0\left[1 + \left(\frac{\lambda_{ex}z}{\pi w_0^2 n}\right)^2\right]^{1/2} \tag{18}$$

and

$$\kappa(z) = 2\int_0^a \frac{d\rho\rho}{R^2(z)} \exp\left[-\frac{2\rho^2}{R^2(z)}\right] = 1 - \exp\left[-\frac{2a^2}{R^2(z)}\right] \tag{19}$$

where the $R(z)$ itself is defined by an expression similar to eq. 18

$$R(z) = R_0\left[1 + \left(\frac{\lambda_{em}z}{\pi R_0^2 n}\right)^2\right]^{1/2} \tag{20}$$

In the above equations, λ_{ex} is the excitation wavelength, and λ_{em} the centre emission wavelength, n is the refractive index of the immersion medium (water), a is the radius of the confocal aperture

divided by magnification, and w_0 and R_0 are two (generally unknown) model parameters. Equation 18 is nothing else than the scalar approximation for the radius of a diverging laser beam with beam waist radius w_0. Equation 17 is a modification of the three-dimensional Gaussian we have already met when discussing one-focus FCS and says that in each plane perpendicular to the optical axis, the MDF is approximated by a Gaussian distribution having width $w(z)$ and amplitude $\kappa(z)/w^2(z)$.

It remains to calculate the auto- and cross-correlation curves of the two-focus set-up. One derives these expressions following a similar philosophy of calculating the photon detection and diffusion probabilities as in the previous section. For example, the (background-free) CCF between the fluorescence signal coming from the two different detection volumes is given by a similar integral as that in eq. 13

$$g\left(\tau,\delta\right) = \frac{c\varepsilon_1\varepsilon_2}{(4\pi D\tau)^{3/2}} \int\limits_V d\mathbf{r}_1 \int\limits_V d\mathbf{r}_0 U(\mathbf{r}_1) \exp\left[-\frac{|\mathbf{r}_1 - \mathbf{r}_0 - \hat{\mathbf{x}}\delta|^2}{4D\tau}\right] U(\mathbf{r}_0) + \varepsilon_1\varepsilon_2 \left[\int\limits_V d\mathbf{r} U(\mathbf{r})\right]^2 \tag{21}$$

Here, we have taken into account that the MDFs of both detection volumes are identical but shifted by a distance δ along the x-axis (along unit vector $\hat{\mathbf{x}}$) and having potentially two different overall detection efficiencies ε_1 and ε_2. Inserting eqs. 17–20 into eq. 21 yields

$$g\left(\tau,\delta\right) = g_\infty(\delta) + \frac{\varepsilon_1\varepsilon_2 c}{4} \sqrt{\frac{\pi}{D\tau}} \int\limits_{-\infty}^{\infty} dz_1 \int\limits_{-\infty}^{\infty} dz_2$$
$$\frac{\kappa(z_1)\kappa(z_2)}{8D\tau + w^2(z_1) + w^2(z_2)} \exp\left[-\frac{(z_2 - z_1)^2}{4D\tau} - \frac{2\delta^2}{8D\tau + w^2(z_1) + w^2(z_2)}\right] \tag{22}$$

which is certainly more complicated than the simple expression of the second line in eq. 13 but not much harder to handle numerically in the age of powerful PCs. For numerical purposes, it is useful to slightly modify this result by changing the variables to

$$\xi = \frac{z_2 - z_1}{2\sqrt{D\tau}}, \eta = \frac{z_2 + z_1}{2} \tag{23}$$

leading to the expression

$$g\left(\tau,\delta\right) = g_\infty(\delta) + 2\varepsilon_1\varepsilon_2 c\sqrt{\pi} \int\limits_0^{\infty} d\xi \int\limits_0^{\infty} d\eta \frac{\kappa\left(\eta - \sqrt{D\tau}\xi\right)\kappa\left(\eta + \sqrt{D\tau}\xi\right)}{8D\tau + w^2\left(\eta - \sqrt{D\tau}\xi\right) + w^2\left(\eta + \sqrt{D\tau}\xi\right)}$$
$$\exp\left[-\xi^2 - \frac{2\delta^2}{8D\tau + w^2\left(\eta - \sqrt{D\tau}\xi\right) + w^2\left(\eta + \sqrt{D\tau}\xi\right)}\right] \tag{24}$$

Because w and κ are rapidly decaying functions for large argument, the infinite integrations over η and ζ can be approximated by numerically evaluating the integrals within a finite two-dimensional strip defined by $|\eta \pm (D\tau)^{1/2}\zeta| < M$, where M is a truncation value chosen in such a way that the numerical integration result does not change when increasing M further. Numerical integration can be done by a simple finite element scheme, and convergence is checked by testing whether the numerical result remains the same upon refining the finite element size and when increasing the threshold value M.

Data fitting is usually performed with least-squares fitting of the model curve, eq. 24, against the measured ACF ($\delta = 0$, $\varepsilon_1\varepsilon_2$ replaced by either ε_1^2 or ε_2^2) and CCF *simultaneously* in a global fit. As fit parameters, one has $\varepsilon_1 c^{1/2}$, $\varepsilon_2 c^{1/2}$, D, w_0 and R_0, as well as three offset values g_∞. The distance δ between the detection regions is determined by the properties of the Nomarski prism and has to be exactly known a priori, thus introducing an external length scale into data evaluation. An elegant and effective way of determining this distance is to perform a comparative measurement of the diffusion of

fluorescently labeled beads with DLS and with 2fFCS [25]. Because both methods have yielded the same value of the diffusion coefficient, one can use the comparison to retrieve the correct interfocal distance. However, to avoid the introduction of systematic errors owing to the finite size of the beads, one should make sure that the bead size is below ~100 nm in diameter [26].

It is important to notice that a crucial criterion-of-fit quality is not only to simultaneously reproduce the temporal shape of both ACFs and the CCF, but also to reproduce their three amplitudes $g_{t \to 0} - g_{\infty}$ using only the two parameters $\varepsilon_1 c^{1/2}$ and $\varepsilon_2 c^{1/2}$. The relation between the amplitudes of the CCF and the amplitudes of the ACFs is determined by the overlap between the two MDFs, and thus by the shape parameters w_0 and R_0. Thus, achieving a good fit quality for the relative amplitudes of the ACFs and the CCF strongly helps to find the correct values of these parameters.

Due to the presence of an external length scale determined by the distance δ between the detection volumes and a reasonably accurate model of the MDF, 2fFCS is indeed a method of superior accuracy and stability for measuring diffusion. An optimal distance between foci is equal to their radius in the focal plane, giving a sufficiently large overlap between detection volumes that the amplitude of the CCF between both detection volumes is roughly one half of the amplitude of each ACF. Larger distances will lead to significantly longer measurement times for accumulating a sufficiently good cross-correlation, smaller distances will lead to a CCF too similar to the ACFs, so that data fitting becomes unreliable.

As was shown in ref. [21], the achievable accuracy of 2fFCS is better than 5 % in absolute value for diffusion measurements. Meanwhile, the method has been used to measure and re-measure the diffusion of several dyes in water throughout the visible spectrum [27,28]. The determined values are reported in Table 1. Remarkably, it has been found that the value of the diffusion coefficient of Rhodamine 6G, which has served for many years as the "golden standard" for calibrating conventional FCS measurements, is by 37 % larger than reported in the literature. However, it should be noted that recently several groups have found similarly large values by using alternative measurement techniques [29,30].

Table 1 Diffusion coefficients of various dyes in aqueous solution.

Dye	λ_{abs}/nm	λ_{abs}/nm	$D_{25°C}$ /(cm$^{-2} \cdot$s^{-1})
Cy5	650	670	$(3.7 \pm 0.15) \cdot 10^{-6}$
Atto655-COOH	665	690	$(4.26 \pm 0.08) \cdot 10^{-6}$
Atto655-maleimide	665	690	$(4.07 \pm 0.1) \cdot 10^{-6}$
Rhodamine 6G	530	560	$(4.14 \pm 0.05) \cdot 10^{-6}$
Oregon Green	488	540	$(4.11 \pm 0.06) \cdot 10^{-6}$

V. CONCLUSIONS AND OUTLOOK

We have mainly considered the application of FCS to diffusion and concentration measurements, which are the most difficult applications in terms of accuracy, reproducibility, and robustness. After discussing the most relevant optical and photophysical artifacts that are troubling standard one-focus FCS, we described the generalized method of 2fFCS, which, for the first time since the invention of FCS, yields accurate and precise results for diffusion coefficients in absolute terms at the infinite-dilution limit. However, it should be noted that even that method, using the improved representation of the MDF as given by eq. 17, yields an estimation of the detection volume (and thus concentration) which can be still inaccurate by more than 100 % in absolute terms. Thus, we still lack a simple and efficient correlation-based method for precise *absolute* concentration measurements in solutions at the pico- to nanomolar concentration level.

However, for *absolute* measurements of diffusion coefficients, 2fFCS is certainly much superior and more accurate than conventional FCS, whereas the technical cost of modifying an existing FCS into

a 2fFCS system is rather moderate. The achievable accuracy of 2fFCS in determining a diffusion coefficient is better than 4 % in absolute numbers. Currently, a first commercial version of a 2fFCS system is already available.

We completely omitted here the application of FCS and related techniques to measure intramolecular dynamics, intermolecular interactions, stoichiometry, or rotational diffusion. A thorough discussion of all these other applications is going much farther than the scope of the present technical note. Also, in all these other applications, the problems discussed here are of no big concern, because the time scale of, for example, intramolecular conformations or rotational diffusion is much faster than the time scale of the diffusive motion within the detection volume, so that the size and shape of the detection volume does not usually have any influence on the correlation curve at these short times. The reader interested in these other applications of FCS is referred to the excellent reviews and books as had been cited in the introduction.

MEMBERSHIP OF SPONSORING BODIES

Membership of the IUPAC Physical and Biophysical Chemistry Division Committee for the period 2012–2013 is as follows:

President: K. Yamanouchi (Japan); *Vice President*: R. Marquardt (France); *Secretary*: A. Wilson (USA); *Past President*: A. McQuillan (New Zealand); *Titular Members*: K. Bartik (Belgium); A. Friedler (Israel); A. Goodwin (USA); R. Guidelli (Italy); A. Russell (UK); J. Stohner (Switzerland); *Associate Members*: V. Barone (Italy); A. Császár (Hungary); V. Kukushkin (Russia); V. Mišković-Stanković (Serbia); Á. Mombrú Rodríguez (Uruguay); X. S. Zhao (China); *National Representatives*: K. Bhattacharyya (India); J. Cejka (Czech Republic); S. Hannongbua (Thailan); M. Koper (Netherlands); A. J. Mahmood (Bangladesh); O. Mamchenko (Ukraine); J. Mdoe (Tanzania); F. Quina (Brazil); N. Soon (Malaysia); V. Tomišić (Croatia).

Membership of the IUPAC Organic and Biomolecular Chemistry Division Committee for the period 2012–2013 is as follows:

President: K. Ganesh (India); *Vice President*: M. Garson (Australia); *Secretary*: A. Griesbeck (Germany); *Past President*: G. Koomen (Netherlands); *Titular Members*: G. Blackburn (UK); A. Brandi (Italy); M. Brimble (New Zealand); T. Carell (Germany); B. Han (China); F. Nicotra (Italy); *Associate Members*: M. Cesa (USA); V. Dimitrov (Bulgaria); H. Jacobs (Jamaica); S. H. Kang (Korea); M. Orfanopoulos (Greece); D. Sladić (Serbia); *National Representatives*: A. Al-Aboudi (Jordan); P. Crowley (Ireland); L. Dias (Brazil); E. Innocent (Tanzania); K. Khan (Pakistan); T. Krygowski (Poland); C.-C. Liao (Taiwan); D. Mizrahi (Israel); J. Streith (France); T. Vilaivan (Thailand).

Membership of the IUPAC Analytical Chemistry Division Committee for the period 2012–2013 is as follows:

President: M. Camões (Portugal); *Vice President*: D. Hibbert (Australia); *Secretary*: Z. Mester (Canada); *Past President*: A. Fajgelj (Austria); *Titular Members*: C. Balarew (Bulgaria); A. Felinger (Hungary); J. Labuda (Slovakia); M. C. Magalhães (Portugal); J. M. Pingarrón (Spain); Y. Thomassen (Norway); *Associate Members*: R. Apak (Turkey); P. Bode (Netherlands); Y. Chen (China); H. Kim (Korea); Y. H. Lee (Malaysia); T. Maryutina (Russia); *National Representatives*: A. Alam (Bangladesh); O. Chande Othman (Tanzania); L. Charles (France); M. Eberlin (Brazil); K. Grudpan (Thailand); J. Hanif (Pakistan); D. Mandler (Israel); P. el Novak (Croatia); H. Sirén (Finland); N. Torto (South Africa).

This document was prepared in the frame of IUPAC Project #2004-021-1-300, Reference Methods, Standards and Applications of Photoluminescence. *Chairs*: Fred Brouwer, Enrique San Román; *Members*: Ulises Acuña, Marcel Ameloot, Noël Boens, Cornelia Bohne, Paul DeRose, Jörg Enderlein, Nikolaus Ernsting, Thomas Gustavsson, Niels Harrit, Johan Hofkens, Alex Knight, Helge

Lemmetyinen, Hiroshi Miyasaka, Ute Resch-Genger, Alan Ryder, Trevor Smith, Mark Thompson, Bernard Valeur, Hiroyuki Yoshikawa.

REFERENCES

1. D. Magde, E. Elson, W. W. Webb. *Phys. Rev. Lett.* **29**, 705 (1972).
2. E. L. Elson, D. Magde. *Biopolymers* **13**, 1 (1974).
3. D. Magde, E. Elson, W. W. Webb. *Biopolymers* **13**, 29 (1974).
4. N. O. Petersen. *Biophys. J.* **49**, 809 (1986).
5. N. O. Petersen, D. C. Johnson, M. J. Schlesinger. *Biophys. J.* **49**, 817 (1986).
6. J. Widengren, Ü. Mets. "Conceptual basis of fluorescence correlation spectroscopy and related techniques as tools in bioscience", in *Single-Molecule Detection in Solution: Methods and Applications*, C. Zander, J. Enderlein, R. A. Keller (Eds.), pp. 69–95, Wiley-VCH, Berlin (2002).
7. P. Schwille. *Cell. Biochem. Biophys.* **34**, 383 (2001).
8. S. T. Hess, S. Huang, A. A. Heikal, W. W. Webb. *Biochemistry* **41**, 697 (2002).
9. R. Rigler, E. Elson (Eds.). *Fluorescence Correlation Spectroscopy*, Springer, Berlin (2001).
10. M. Böhmer, J. Enderlein. "Single molecule detection on surfaces with the confocal laser scanning microscope", in *Single-Molecule Detection in Solution: Methods and Applications*, C. Zander, J. Enderlein, R. A. Keller (Eds.), pp. 145–183, Wiley-VCH, Berlin (2002).
11. J. Enderlein, F. Pampaloni. *J. Opt. Soc. Am. A* **21**, 1558 (2004).
12. M. Wahl, I. Gregor, M. Patting, J. Enderlein. *Opt. Expr.* **11**, 3583 (2003).
13. A. Einstein. *Investigations on the Theory of the Brownian Movement*, Dover, New York (1985).
14. A. M. Weljie, A. P. Yamniuk, H. Yoshino, Y. Izumi, H. J. Vogel. *Protein Sci.* **12**, 228 (2003).
15. B. J. Berne, R. Pecora. *Dynamic Light Scattering*, Dover, New York (2000).
16. P. T. Callaghan. *Principles of Nuclear Magnetic Resonance Microscopy*, Clarendon Press, Oxford (1991).
17. D. Harvey. *Modern Analytical Chemistry*, pp. 593–595, McGraw-Hill, Boston (2000).
18. J. L. Cole, J. C. Hansen. *J. Biomol. Technol.* **10**, 163 (1999).
19. W. Liu, T. Cellmer, D. Keerl, J. M. Prausnitz, H. W. Blanch. *Biotechnol. Bioeng.* **90**, 482 (2005).
20. T. Kiefhaber, R. Rudolph, H. H. Kohler, J. Buchner. *Nat. Biotechnol.* **9**, 825 (1991).
21. J. Enderlein, I. Gregor, D. Patra, T. Dertinger, B. Kaupp. *ChemPhysChem* **6**, 2324 (2005).
22. J. Enderlein. *Chem. Phys. Lett.* **410**, 452 (2005).
23. T. Dertinger, V. Pacheco, I. von der Hocht, R. Hartmann, I. Gregor, J. Enderlein. *ChemPhysChem* **8**, 433 (2007).
24. B. K. Müller, E. Zaychikov, C. Bräuchle, D. C. Lamb. *Biophys. J.* **89**, 3508 (2005).
25. C. B. Müller, K. Weiß, W. Richtering, A. Loman, J. Enderlein. *Opt. Expr.* **16**, 4322 (2008).
26. C. B. Müller, A. Loman, W. Richtering, J. Enderlein. *J. Phys. Chem. B* **112**, 8236 (2008).
27. A. Loman, T. Dertinger, F. Koberling, J. Enderlein. *Chem. Phys. Lett.* **459**, 18 (2008).
28. C. B. Müller, A. Loman, V. Pacheco, F. Koberling, D. Willbold, W. Richtering, J. Enderlein. *Eur. Phys. Lett.* **83**, 46001 (2008).
29. C. T. Culbertson, S. C. Jacobson, J. M. Ramsey. *Talanta* **56**, 365 (2002).
30. Z. Petrasek, P. Schwille. *Biophys. J.* **94**, 1437 (2008).